Microdosimetry in a realistic keratinocyte cell model at mmWave and HF frequencies

Zain Haider*[(1)], Yves Le Dréan [(2)], Ronan Sauleau[(1)], Laura Caramazza[(3)], Micaela Liberti[(3)], and Maxim Zhadobov[(1)]
(1) Univ Rennes, CNRS, Institut d'Électronique et des Technologies du numéRique, UMR 6164, F-35000, Rennes, France
(2) Univ Rennes, Inserm, Institut de Recherche en Santé, Environnement et Travail-UMR_S 1085, F-35000 Rennes, France.
(3) Department of Information Engineering, Electronics and Telecommunications (DIET), Sapienza University of Rome, 00185 Rome, Italy

Abstract

Wide spread of millimeter-wave (mmWave) and wireless power transfer (WPT) technologies opens new challenges in terms of characterization of bioelectromagnetic interactions. The objective of this study is to investigate quantitatively the induction of such electromagnetic radiation within cells at 6.78 MHz and 60 GHz respectively. A realistic model of the keratinocyte, which takes into account the complex morphologies and volume fraction of organelles, was developed. The finite element method (FEM) was used to solve the Laplace's equation under quasi-static approximation. The results show that the power loss density (PLD) within the cellular and subcellular compartments increases with frequency due to diminished shielding effect of the membranes. At 60 GHz and 6.78 MHz, the average power loss density (PLD_{avg}) within the cellular and subcellular organelles is about six and three orders of magnitude higher than that at 1 kHz. Also, in comparison to the background PLD_{avg} within cytoplasm (CP), the intracellular traffic through the nuclear pores (N_p) is submitted to three orders of magnitude higher exposure level at 6.78 MHz and 2.5 times higher exposure level at 60 GHz.

1 Introduction

There has been a tremendous growth in mobile data traffic over the past few years. According to Cisco, the mobile data traffic is expected to grow by 46% annually between 2017 and 2022 [1]. The exponential increase in demand for mobile data is due to rise in use of mobile multimedia services. However, the primary challenge limiting growth of wireless communications is scarcity of microwave spectrum. The incredible demand for the high data rate can be met by using huge untapped bandwidth resources of the millimeter-wave (mmWave) spectrum. The mmWave technologies are also envisioned to be the key enabling technology for the forthcoming fifth generation (5G) cellular systems dawning a new era of wireless connectivity anytime and anywhere [2]. Concurrently, the interest in charging devices wirelessly is also growing at a rapid pace. The Qi (100-205 kHz) and Airfuel (277-357 kHz & 6.78 MHz) are the two rival interface standards developed for near-field wireless power transfer (WPT) systems [3].

The rapid advancements in mmWave and WPT technolo--gies have been raising concern among general public regarding the safety of such electromagnetic (EM) exposure. Analytical [4], circuital [5] and numerical methods [6] have been utilized to calculate dosimetric quantities at the cellular level. Moreover, in order to accurately predict microscopic non-uniformity in electric field in the high frequency regime, dielectric relaxation of membranes and water molecules is also taken into account in [7] by using Debye dispersion relation. In this study, the absorption electromagnetic radiation is quantified for a realistic cell model with a special focus at mmWave band (60 GHz) and high frequency band (HF) upcoming for WPT (6.78 MHz).

2 Material and Methods
2.1 Cell Geometric Model

The electron microscopy image of the basal keratinocyte given in [8] was utilized to construct the geometric model as shown in Figure 1(a). The length of the keratinocyte is ~14 μm [9] and plasma membrane (P_m) with a thickness of 5 nm surrounds the cell. The organelle volume percentage data for basal keratinocytes was taken from [10] and spherical approximation was used to convert it to 2D surface area.

2.1.1 Nucleus

The nucleus of the basal keratinocytes is represented by an ellipse with a minor and major radius of 2.1 μm and 3.5 μm respectively as displayed in Figure 1 (a). Two 5 nm thick membranes along with an intermembrane distance (N_{ims}) of 60 nm form an envelope around the nucleus interior (N_i) [11]. The nuclear envelope is perforated by nine nuclear pores (N_p). The thickness of each nuclear pore is roughly 9 nm [12]. In a typical 2D cross section (hereinafter referred to as cell surface area) of a basal keratinocyte, the nucleus occupies roughly 26.3% of the surface area.

2.1.2 Mitochondria

The mitochondrion has nearly an elliptical structure with minor and major radius of 0.1 μm and 0.3 μm respectively as shown in Figure 1 (b) [11]. The lumen of mitochondria
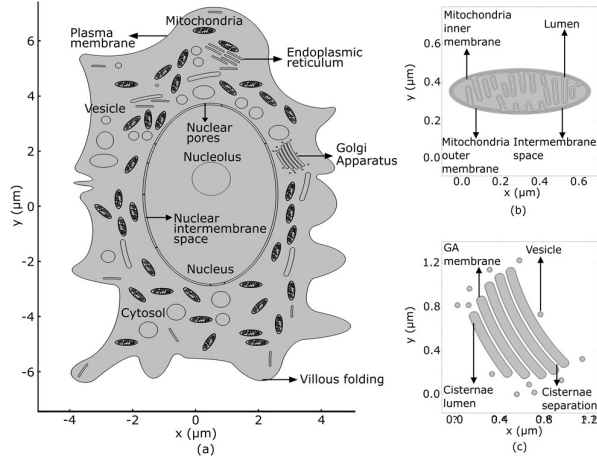
Figure 1. 2D geometric model (a) keratinocyte (b) mitochondria (c) Golgi apparatus

(M_L) is limited by two 7 nm thick lipid bilayer membranes with an intermembrane distance (M_{ims}) of 6 nm [13]. The inner membrane of mitochondria (M_{im}) is arranged in many folds (cristae). The cristae are up to 100 nm long and roughly 27 nm wide. The mitochondrion is designed based on electron microscopy image given in [14] and comprises roughly 4.6% of cell surface area.

2.1.3 Endoplasmic reticulum

The endoplasmic reticulum (ER) consists of a network of elongated tubules, which are surrounded by a 5 nm thick membrane as shown in Figure 1. The length of the tubules ranges from 0.4-1 μm and width of their lumen (ER_L) is roughly 50-150 nm [15]. The ER of basal keratinocytes occupies only 1.5% of cell surface area as these cells are not involved in secretions.

2.1.4 Golgi apparatus

Golgi apparatus (GA) is composed of five layers of elongated sacs limited by a 5 nm thick membrane as displayed in Figure 1(c). The length of sacs ranges from 0.5-1 μm [16] and the thickness of their lumen (GA_L) is typically 90 nm [11]. The distance between the adjacent sacs is roughly 20 nm [17]. The GA is positioned on right side of the nucleus. There are also several 50 nm vesicles around the GA. In basal keratinocytes, GA occupies 0.5% of cell surface area.

2.1.4 Other Organelles

The melanosomes, membrane coating granules, secretory vesicles and lysosomes are represented by circles and ellipses with a radius between 25-450 nm [11]. The interior of these organelles (V_L) is also surrounded by a 5 nm thick membrane. These organelles occupy roughly 3.6% of cell surface area and are arranged randomly within cytoplasm (CP) as shown in Figure 1(a).

2.2 Cell Dielectric Model

The frequency dependent dielectric properties of the membranes and cellular compartments based on Debye model were taken from literature and are reported in Table 1.

$$\varepsilon^*(f) = \frac{\sigma}{j\varepsilon_0 2\pi} + \frac{\varepsilon_S - \varepsilon_\infty}{1 + jf/f_{relax}} + \varepsilon_\infty, \qquad (1)$$

where σ is the conductivity, ε_s is the static permittivity, ε_∞ is the optical permittivity, and f_{relax} is the relaxation frequency.

2.3 Numerical Method

The AC/DC module of COMSOL Multiphysics 5.5 based on finite element method (FEM) was used to perform the numerical simulations in the frequency range between 1 kHz and 100 GHz. The Laplace's equation was solved under quasi-static approximation. The keratinocyte cell model was placed in the computational domain with the dimensions of 40 μm x 40 μm. The electric potential boundary condition with 40 μV was applied to the upper boundary while ground was applied to the lower boundary of the computational domain to expose the cell to an electric field of 1 V/m. On the remaining boundaries, the electric insulation conditions were assigned.

3 Results
3.1 Frequency dependent response

The average power loss density (PLD_{avg}) inside the interior of all cellular compartments is lower than 19.8 μW/m³ at 1 kHz as shown in Figure 2. The lower PLD_{avg} is because of the shielding effect of the cellular and subcellular membranes. As shown in Figure 2, the PLD_{avg} inside the organelles and CP rises with the increase of frequency between 1 kHz and 10 MHz. The increase in PLD_{avg} is due

Table 1
Debye Models of Cellular Compartments

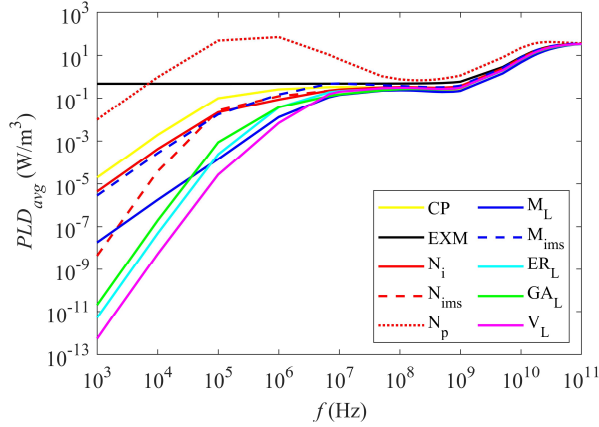| Compartment	ε_s	ε_∞	f_{relax}	σ (S/m)
Plasma membrane [6]	12.27	1.92	325.60 MHz	10^{-7}
Subcellular membranes [7]	11.7	4	179.85 MHz	1.1×10^{-7}
Outer mitochondria membrane (M_{om}) [7], [18]	11.7	4	179.85 MHz	1×10^{-4}
Extracellular medium (EXM) [19]	76	6.9	18.5 GHz	1
Cytoplasm (CP) [7], [20]	67	5	17.9 GHz	0.32
Organelle lumen [7]	67	5	17.9 GHz	0.55

Figure 2. Frequency dependent response of cellular compartments

to the weakened shielding effect of the membranes caused by their dielectric relaxation in the MHz range. Particularly, at 6.78 MHz, PLD_{avg} is 0.33 W/m^3 in CP, 0.229 W/m^3 in N_i, 0.227 W/m^3 in N_{ims}, 0.190 W/m^3 in ER_L, 0.127 W/m^3 in GA_L, 0.479 W/m^3 in M_{ims}, 0.11 W/m^3 in M_L, 0.15 W/m^3 in V_L and 0.482 W/m^3 in EXM. Note that the PLD_{avg} within the nuclear pores is higher than rest of the cellular compartments in the 10 kHz-10 MHz frequency range. The PLD_{avg} within all cellular compartments reaches a plateau between 10 MHz to 1 GHz. However, above 5 GHz the PLD_{avg} within cellular compartments increases swiftly due to the dielectric relaxation of water molecules. Specifically, at 60 GHz, PLD_{avg} is 32.04 W/m^3 in CP, 31.716 W/m^3 in N_i, 31.676 W/m^3 in N_{ims}, 39.008 W/m^3 in N_p, 30.29 W/m^3 in ER_L, 30.67 W/m^3 in GA_L, 33.62 W/m^3 in M_{ims}, 29.34 W/m^3 in M_L, 31.478 W/m^3 in V_L and 32.68 W/m^3 in EXM.

3.2   Local Power Absorption

Figure 3 and Figure 4 show that power loss density (PLD)
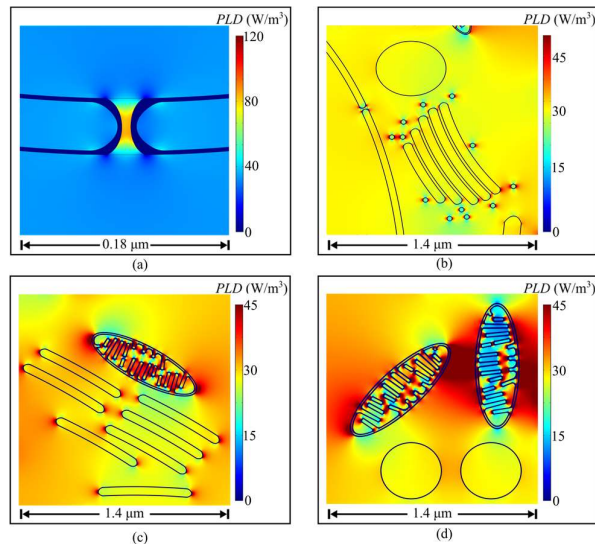

Figure 3. PLD at 60 GHz (a) nuclear pores (b) Golgi apparatus (c) ER (d) mitochondria
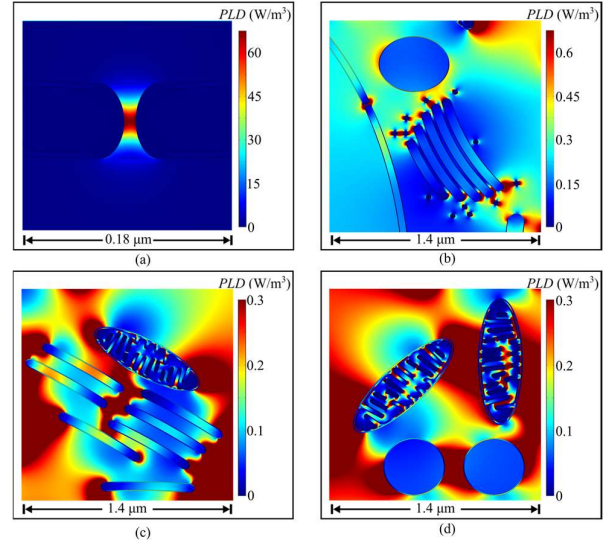

Figure 4. PLD at 6.78 MHz (a) nuclear pores (b) Golgi apparatus (c) ER (d) mitochondria

within various cellular compartments at 6.78 MHz and 60 GHz is non-uniform. The PLD inside the N_p is higher than the background PLD_{avg} in CP by roughly three orders of magnitude at 6.78 MHz and 2.5 times at 60 GHz as shown in Figure 3(a) and Figure 4(a). Also, the PLD within various cellular compartments depends on their size. The PLD within the smaller membrane bound vesicles shown in Figure 3(b) and Figure 4(b) is 35 times and 1.2 times lower than that of larger membrane bound sacs of GA at 6.78 MHz and 60 GHz respectively. The arrangement of the organelles within the cell also plays an important role in determining the PLD inside them. For instance, the ER tubules which are below the mitochondria in the Figure 3(c) and Figure 4(c) exhibit roughly two times and 1.2 times lower PLD than ER tubules which are not completely shielded by the mitochondria at 6.78 MHz and 60 GHz respectively. Finally, the maximum PLD in the small gap between the two mitochondria shown in Figure 3(d) and Figure 4(d) is roughly 5 times and 1.6 times higher than the background PLD_{avg} in CP at 6.78 MHz and 60 GHz respectively.

4   Conclusion

The power losses within the cellular compartments increase with frequency due to the weakened shielding effect of the cellular and subcellular membranes. At 60 GHz and 6.78 MHz, the average power loss density (PLD_{avg}) within the cellular and subcellular organelles is about six and three orders of magnitude higher than that at 1 kHz. The results also show that position and arrangement of organelles within the cell play an important role in determining the local power absorption inside the cell. Also, higher power absorption within the nuclear pores (N_p) suggests that intracellular traffic is submitted to higher absorption in comparison to the background absorption within the cytoplasm (CP).

5 Acknowledgement

6 References

1. Cisco Visual Networking Index: Global Mobile Data Traffic Forecast Update 2017–2012 White Paper, https://www.cisco.com/c/en/us/solutions/collateral/service-provider/visual-networking-index-vni/white-paper-c11-738429.html.

2. Y. Zeng and R. Zhang, "Millimeter wave MIMO with lens antenna array: A new path division multiplexing paradigm," IEEE Trans. Commun., vol. 64, no. 4, Apr. 2016, pp. 1557-1571, https://doi.org/10.1109/TCOMM.2016.2533490.

3. W. Jin, A. T. L. Lee, S.-C. Tan, and S. Y. Hui, "A Gallium Nitride (GaN)-Based Single-Inductor Multiple-Output (SIMO) Inverter with Multi-Frequency AC Outputs," *IEEE Trans. Power Electron.*, vol. 34, no. 11, Nov. 2019, pp. 10856–10873, doi: 10.1109/TPEL.2019.2896649.

4. T. Kotnik and D. Miklavcic, "Second-order model of membrane electric field induced by alternating external electric fields," *IEEE Trans. Biomed. Eng.*, vol. 47, no. 8, Aug. 2000, pp. 1074–1081, doi: 10.1109/10.855935.

5. C. Merla *et al.*, "Novel Passive Element Circuits for Microdosimetry of Nanosecond Pulsed Electric Fields," *IEEE Trans. Biomed. Eng.*, vol. 59, no. 8, Aug. 2012, pp. 2302–2311, doi: 10.1109/TBME.2012.2203133.

6. C. Merla, M. Liberti, F. Apollonio, C. Nervi, and G. d'Inzeo, "A 3-D microdosimetric study on blood cells: A permittivity model of cell membrane and stochastic electromagnetic analysis," *IEEE Trans. Microw. Theory Tech.*, vol. 58, no. 3, Mar. 2010, pp. 691–698, https://doi.org/10.1109/TMTT.2010.2040338.

7. C. Merla, M. Liberti, F. Apollonio, and G. d'Inzeo, "Quantitative assessment of dielectric parameters for membrane lipid bi-layers from RF permittivity measurements," *Bioelectromagnetics*, vol. 30, no. 4, May 2009, pp. 286–298, doi: 10.1002/bem.20476.

8. W. Montagna and P. F. Parakkal, "The epidermis," in The Structure and Function of Skin, 3rd ed., New York: Academic Press, 1974, pp. 28.

9. T.-T. Sun and H. Green, "Differentiation of the epidermal keratinocyte in cell culture: Formation of the cornified envelope," Cell, vol. 9, no. 4, Dec. 1976, pp. 511–521, https://doi.org/10.1016/0092-8674(76)90033-7.

10. A. J. P. Klein-Szanto, "Stereological baseline data of normal human epidermis," J. Invest. Dermatol., vol. 68, no. 2, Feb. 1977, pp. 73–78, https://doi.org/10.1111/1523-1747.ep12491611.

11. A. S. Zelickson and J. F. Hartmann, "An electron microscopic study of human epidermis," J. Invest. Dermatol., vol. 36, no. 2, Feb. 1961, pp. 65–72, https://doi.org/10.1038/jid.1961.14.

12. J. E. Hall, Guyton and Hall textbook of medical physiology, 12th ed. Philadelphia, PA: Elsevier, 2016, pp. 17.

13. M. H. Ross and W. Pawlina, Histology: A Text and Atlas: With Correlated Cell and Molecular Biology, 7th ed., Lippincott Williams & Wilkins, 2016, pp. 52-82.

14. T. G. Frey and C. A. Mannella, "The internal structure of mitochondria," Trends Biochem. Sci., vol. 25, no. 7, Jul. 2000, pp. 319–324, https://doi.org/10.1016/S0968-0004(00)01609-1.

15. M. Terasaki et al., "Stacked endoplasmic reticulum sheets are connected by helicoidal membrane motifs," Cell, vol. 154, no. 2, Jul. 2013, pp. 285–296, https://doi.org/10.1016/j.cell.2013.06.031.

16. D. J. Morré and H. H. Mollenhauer, "Structure," in The Golgi apparatus: the first 100 years, New York: Springer, 2009, pp. 12.

17. R. S. Polishchuk and A. A. Mironov, "Structural aspects of Golgi function," Cell. Mol. Life Sci. CMLS, vol. 61, no. 2, Jan. 2004, pp. 146–158, https://doi.org/10.1007/s00018-003-3353-8.

18. H. Qiu, S. Xiao, and R. P. Joshi, "Simulations of voltage transients across intracellular mitochondrial membranes due to nanosecond electrical pulses," *IEEE Trans. Plasma Sci.*, vol. 42, no. 10, Oct. 2014, pp. 3113–3120, https://doi.org/10.1109/TPS.2014.2308871.

19. M. Casciola, M. Liberti, A. Denzi, A. Paffi, C. Merla, and F. Apollonio, "A computational design of a versatile microchamber for in vitro nanosecond pulsed electric fields experiments," *Integration*, vol. 58, Jun. 2017, pp. 446–453, https://doi.org/10.1016/j.vlsi.2017.03.005.

20. Denzi *et al.*, "Assessment of cytoplasm conductivity by nanosecond pulsed electric fields," *IEEE Trans. Biomed. Eng.*, vol. 62, no. 6, Jun. 2015, pp. 1595–1603, https://doi.org/10.1109/TBME.2015.2399250.